Compensating for Fingertip Size to Render Tactile Cues More Accurately

Eric M Young, David Gueorguiev, Katherine J Kuchenbecker, Claudio Pacchierotti

Compensating for Fingertip Size to Render Tactile Cues More Accurately

Eric M. Young, David Gueorguiev, Katherine J. Kuchenbecker*, and Claudio Pacchierotti*

***Abstract*—Fingertip haptic feedback offers advantages in many applications, including robotic teleoperation, gaming, and training. However, fingertip size and shape vary significantly across humans, making it difficult to design fingertip interfaces and rendering techniques suitable for everyone. This paper starts with an existing data-driven haptic rendering algorithm that ignores fingertip size, and it then develops two software-based approaches to personalize this algorithm for fingertips of different sizes using either additional data or geometry. We evaluate our algorithms in the rendering of pre-recorded tactile sensations onto rubber casts of six different fingertips as well as onto the real fingertips of 13 human participants. Results on the casts show that both approaches significantly improve performance, reducing force error magnitudes by an average of 78% with respect to the standard non-personalized rendering technique. Congruent results were obtained for real fingertips, with subjects rating each of the two personalized rendering techniques significantly better than the standard non-personalized method.**

I. Introduction

THE fingertip has always been considered a privileged target for haptic interfaces, including many recently-developed wearable haptic displays [1]. Designing fingertip interfaces that fit all users is challenging; many studies have highlighted large differences in the fingertip's size across the human population. Dandekar et al. [2] assert that the human index fingertip varies between 16 and 20 mm in width, while Johnson and Blackstone [3] registered a width of 20.3 ± 2.4 mm (mean $\pm$ standard deviation) for the same finger across participants. Gender, race, and age all play a role in causing these differences [4], [5], [6]. Moreover, the five fingertips on a single hand vary greatly in size and shape. These physical differences between fingertips have the potential to distort the perception of haptic feedback provided by fingertip haptic devices. Indeed, touch is highly sensitive to variations in contact stimulation, such as small changes of the contact force during static [7] and dynamic touch [8]. Viscoelastic models are often used to describe the fingertip [9], [10], although meaningful tactile interactions have been rendered by fingertip haptic devices even when dynamic components of the interaction, such as velocity and acceleration, are ignored [11], [12]. It has also been shown that realistic force rendering is more important that the geometry of the explored feature [13], [14], and that users will optimally adjust their normal and tangential force during a haptic task to increase their sensitivity [15]. In addition, the rendered contact forces play a key role in performing efficient motor control. If humans cannot rely on haptic feedback, they tend to overtighten their grip [16], [17], which can tire the user and damage the item being grasped.

E. M. Young is with the Mechanical Engineering and Applied Mechanics Department, University of Pennsylvania – Philadelphia, USA, and with the Haptic Intelligence Department, Max Planck Institute for Intelligent Systems – Stuttgart, Germany (e-mail: yoeric@seas.upenn.edu).

D. Gueorguiev and K. J. Kuchenbecker are with the Haptic Intelligence Department, Max Planck Institute for Intelligent Systems – Stuttgart, Germany (e-mails: dgueorguiev@is.mpg.de, kjk@is.mpg.de)

C. Pacchierotti is with CNRS, Univ Rennes, Inria, IRISA – Rennes, France (e-mail: claudio.pacchierotti@irisa.fr).

* These two authors contributed equally to this work.

The authors would like to thank Ruben Werbke for his help in 3D-printing the components, and Ad Spiers and Saekwang Nam for guidance in molding techniques and material selection. E. M. Young is supported by the NSF Graduate Research Fellowship Program under Grant No. DGE-1321851.

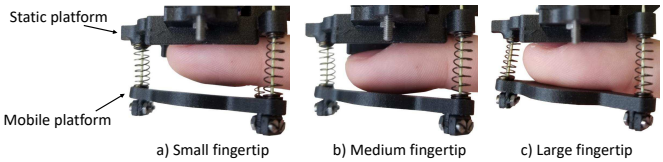

Fig. 1. Problem: the same end-effector configuration elicits different sensations for fingertips of different size, including users with (a) small, (b) medium, and (c) large fingertips. Our personalization methods aim to account for the user's fingertip shape so as to always elicit the desired haptic sensation.

Given the high variability of human fingertip characteristics and the human tactile sensitivity to contact sensations, we strongly believe the unique characteristics of each fingertip should be taken into account when designing fingertip interfaces and rendering algorithms (see Fig. 1). A recent study showed that the size of the user's finger influenced their ability to accurately perceive haptic cues rendered the same way for everyone [18]. In another work on tactile rendering for the fingertip, Pacchierotti et al. [11] hypothesized that recalibrating their algorithm for different fingertip sizes would improve the quality of the rendering across individuals. However, traditionally, haptic rendering algorithms have been designed without accounting for finger size, incorrectly assuming that the provided sensations would be (roughly) consistent across users.

A few approaches partially take this important variable into account by implementing closed-loop control via a force or pressure sensor. For example, the wearable fingertip device of Chinello et al. [19] used three force-sensing resistors (FSRs) to register the contact sensations applied by the end-effector onto the finger skin. By closing a force-control loop around these sensor readings, this device was able to adapt to fingertips of different shapes. Leonardis et al. [20] placed an OptoForce three-axis optical force sensor on the end-effector of their wearable fingertip device. However, they used it only to characterize the force-indentation response of the device, and they did not look into personalization for individual users.

Others have used open-loop force output to render appropriate sensations to differently sized fingertips. For example, Solazzi et al. [21] presented a 3-DoF device that uses two position-controlled actuators to locate a platform around the fingertip and one force-controlled voice coil actuator to render forces into the fingertip. The current commanded to the voice coil was proportional to the force acting on a finger avatar moving in a virtual environment. Similarly, Khurshid et al. [22] rendered one-dimensional haptic feedback to the operator's fingertip via a voice coil whose current was proportional to the force experienced at the robot's side.

Although both force feedback approaches address personalization, each comes with limitations. Closed-loop force control inevitably makes the overall system bulkier, as a sensor must be included on the device. Furthermore, force control enters into play only *after* the end-effector contacts the skin, and it is thus not able to control the position and orientation of the end-effector at the moment of contact, nor the precise timing of initial contact. Finally, both approaches require an interpretable desired force that some tactile sensors, such as the SynTouch BioTac, do not directly provide [23]. This paper proposes two methods to overcome these limitations and personalize the haptic

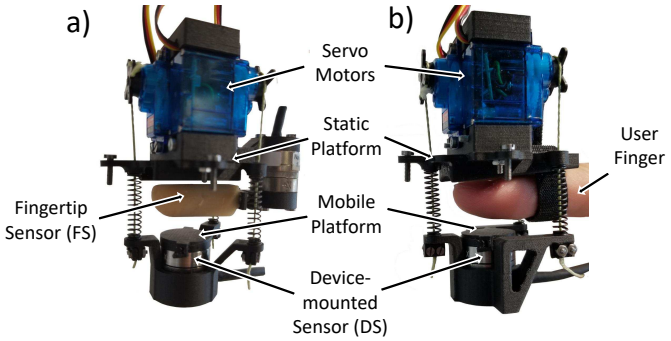

Fig. 2. Our 3-DoF fingertip device modified to house a device-mounted sensor (DS) on the mobile platform. This sensor is needed only during the data collection phase. The device is shown being worn by (a) our fingertip sensor (FS) and (b) a human user. The FS is suspended in the device such that any force exerted by the mobile platform is fully transferred into the sensor.

rendering algorithm of a fingertip haptic device for fingertips of different size. Each algorithm has unique benefits and drawbacks; they both modify a known data-driven rendering algorithm, changing its core characteristics to account for the geometry of a target fingertip, and they are compatible with any mechanical design of a fingertip device and any fingertip sensor. To the best of our knowledge, we are the first to directly address the issue of personalization in fingertip haptics.

II. Context and System

A. Fingertip device and sensor design

For this work, we chose a three-degree-of-freedom (3-DoF) fingertip device similar to that of [11], [12], [24] and shown in Figs. 1 and 2. It is composed of a static platform grounded on the back of the fingertip and a moving platform located opposite the fingertip and acting as the end-effector. The two platforms are connected by three cables enclosed by three springs, each of which is driven by a servo motor (HS-55) mounted to the static platform. The device is able to provide the sensations of making and breaking contact with slanted surfaces as well as pressing on them. We also built a modified version of this device that is able to house a device-mounted sensor (DS), in our case a Nano17 force/torque sensor, on the mobile platform (see Fig. 2). This additional sensor is required for our data-driven personalization approach, which will be discussed in Section III-A.

Similar to [11], [12], we use a fingertip-shaped sensor (FS) to record remote and rendered interactions. It consists of a 3D-printed rigid core attached to an ATI Nano17 sensor on one side and embedded in a VytaFlex rubber fingertip cast on the other (see Fig. 3). The tip of our FS is a quarter sphere with a radius of 7.5 mm; it registers six-dimensional force/torque readings. Although existing sensors offer greater sensing richness, our evaluation presented in Sec. IV required us to create a fingertip sensor with custom geometry, leading us to choose this sensor setup instead. Even though we present and test our two personalization approaches using the above haptic system, both are compatible with any other similar fingertip device and sensor.

B. The standard data-driven rendering algorithm

We start from the standard data-driven haptic rendering algorithm presented by Pacchierotti et al. [12]. Although this algorithm ignores the viscoelastic components of the fingertip response, prior work showed that the interaction sequences generated by the algorithm received high ratings from participants. They used a setup similar to ours, with a 3-DoF fingertip device and a fingertip-like BioTac sensor. First, the BioTac sensor is placed inside the fingertip device in the same way a human user would wear it (similar to Fig. 2a). Then, the end-effector of the device is moved to a wide range of configurations,

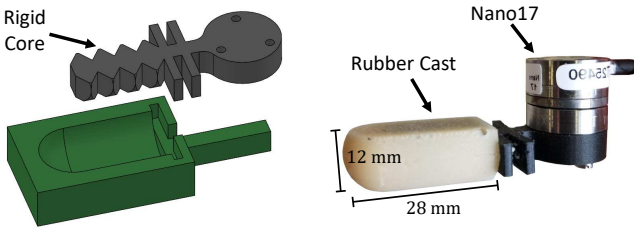

(a) Mold used to shape the FS. (b) The complete FS.

Fig. 3. Our fingertip-shaped sensor (FS) consists of a 3D-printed rigid core attached to an ATI Nano17 force/torque sensor on one side and embedded in a molded VytaFlex rubber fingertip-like cast on the other.

and the effect of each of these configurations is measured by the sensor. This data collection process generates a lookup table, expressed with a mapping function

$$\mu(\mathbf{f}_*) = \mathbf{m}_*, \tag{1}$$

where $\mathbf{m}_*$ is a vector of motor inputs (three, in this case) commanded during the data collection process and $\mathbf{f}_*$ is the corresponding fingertip sensor outputs (twenty, in the case of the BioTac, and six for our FS).

To render a new tactile sensation $\mathbf{f}$ registered by the sensor in a remote environment, Pacchierotti et al. [12] searched the lookup table to find the n most similar sensor outputs measured during data collection, $\widetilde{\mathbf{f}}_*$. Let us define this search function as

$$\nu_n(\mathbf{f}) = \begin{bmatrix} \mathbf{f}_{*,1} & \cdots & \mathbf{f}_{*,n} \end{bmatrix}^T = \widetilde{\mathbf{f}}_*. \tag{2}$$

They then mapped each element of $\widetilde{\mathbf{f}}_*$ back to its corresponding motor inputs, using the lookup table,

$$\mu_n(\widetilde{\mathbf{f}}_*) = \mu_n\left(\begin{bmatrix} \mathbf{f}_{*,1} \\ \vdots \\ \mathbf{f}_{*,n} \end{bmatrix}\right) = \begin{bmatrix} \mu(\mathbf{f}_{*,1}) \\ \vdots \\ \mu(\mathbf{f}_{*,n}) \end{bmatrix} = \begin{bmatrix} \mathbf{m}_{*,1} \\ \vdots \\ \mathbf{m}_{*,n} \end{bmatrix} = \widetilde{\mathbf{m}}_*. \tag{3}$$

Finally, the n motor inputs $\widetilde{\mathbf{m}}_*$ were averaged into one, weighting each input $\mathbf{m}_{*,i}$ according to the distance between the original sensation $\mathbf{f}$ and the one elicited by $\mathbf{m}_{*,i}$ during data collection, $\mathbf{f}_{*,i}$ [12],

$$\varphi_n(\widetilde{\mathbf{m}}_*) = \varphi_n\left(\begin{bmatrix} \mathbf{m}_{*,1} & \cdots & \mathbf{m}_{*,n} \end{bmatrix}^T\right) = \widehat{\mathbf{m}}, \tag{4}$$

where $\widehat{\mathbf{m}}$ are the final motor commands, expected to recreate $\mathbf{f}$ on the user's fingertip. The final mapping, from a generic sensor sensation $\mathbf{f}$ to the device's motor inputs $\widehat{\mathbf{m}}$, is

$$\Lambda_n(\mathbf{f}) = \varphi_n(\mu_n(\nu_n(\mathbf{f}))) = \varphi_n(\mu_n(\widetilde{\mathbf{f}}_*)) = \varphi_n(\widetilde{\mathbf{m}}_*) = \widehat{\mathbf{m}}. \tag{5}$$

Although this algorithm showed good performance [12] and was also employed in a robot-assisted palpation task [11], it has one major drawback; it assumes that the user's fingertip is shaped exactly like the sensor used during the data collection, i.e., the BioTac in their case. As such, the more the user's fingertip differs from the BioTac, the worse the algorithm performs. A representative example of this behavior is shown in Fig. 1.

III. Approaches for Personalization

We aim to personalize the lookup table described above, so as to account for the unique shape of each user's fingertip. We propose two approaches, each with its benefits and drawbacks. Fig. 4 shows the block diagrams summarizing the standard non-personalized approach and our two adjustments. A video explaining our setup, methods, and results is included in the supplemental material; it is also available at https://youtu.be/LlgDyxDT7sg.

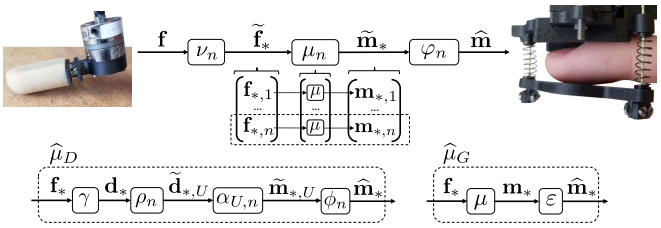

Fig. 4. Block diagrams of all three discussed rendering approaches. The adjustment for data-driven personalization is given by $\widehat{\mu}_D$ and the adjustment for geometric personalization is given by $\widehat{\mu}_G$. In our implementation, $n = 8$, $\mathbf{f}, \mathbf{f}_*, \mathbf{d}_* \in \mathbb{R}^6$, and $\mathbf{m}_*, \widehat{\mathbf{m}}, \widehat{\mathbf{m}}_* \in \mathbb{R}^3$.

A. Data-driven personalization

We start by using our haptic setup to run an FS-centered data collection, similar to what we described in Sec. II-B. The FS is placed inside the device, and DS is placed on the mobile platform, as shown in Fig. 2a. Then, we move the end-effector of the device to a wide range of configurations, and the effect of each of these configurations is registered on the two sensors (FS and DS). We can now define mapping a function similar to eq. (1),

$$\gamma(\mathbf{f}_*) = \mathbf{d}_*, \tag{6}$$

where $\mathbf{f}_* \in \mathbb{R}^6$ is an FS output and $\mathbf{d}_* \in \mathbb{R}^6$ is the corresponding DS output, both measured for each motor configuration $\mathbf{m}_* \in \mathbb{R}^3$.

To enable personalization, we carry out a second, user-centered data collection routine. We remove the FS and ask the target user to wear the device, as shown in Fig. 2b. Then, we move the end-effector of the device to a second wide range of configurations, and we record the effect of each of these configurations using the DS. To spare the user's time, the user-centered data collection can include a smaller set of configurations than the FS-centered data collection. From this second data collection, we define our user personalization function as

$$\alpha_U(\mathbf{d}_{*,U}) = \mathbf{m}_{*,U}, \tag{7}$$

where $\mathbf{m}_{*,U}$ is a vector of motor inputs and $\mathbf{d}_{*,U}$ is the corresponding sensation registered by the DS, for a particular user, U.

Now we have all the information needed to adjust the lookup table defined by eq. (6) for our target fingertip. To do so, for each DS sensation registered during the FS-centered data collection $\mathbf{d}_*$, we find the n nearest DS sensations observed during the user-centered data collection $\widetilde{\mathbf{d}}_{*,U}$, i.e.,

$$\rho_n(\mathbf{d}_*) = \left(\begin{bmatrix} \mathbf{d}_{*,U,1} & \dots & \mathbf{d}_{*,U,n} \end{bmatrix}^T \right) = \widetilde{\mathbf{d}}_{*,U}, \tag{8}$$

and then we retrieve the corresponding motor inputs, defining

$$\alpha_{U,n}(\widetilde{\mathbf{d}}_{*,U}) = \begin{bmatrix} \alpha_U(\mathbf{d}_{*,U,1}) \\ \vdots \\ \alpha_U(\mathbf{d}_{*,U,n}) \end{bmatrix} = \begin{bmatrix} \mathbf{m}_{*,U,1} \\ \vdots \\ \mathbf{m}_{*,U,n} \end{bmatrix} = \widetilde{\mathbf{m}}_{*,U} \tag{9}$$

as the function that maps a set of n DS sensations registered during the user-centered data collection $\widetilde{\mathbf{d}}_{*,U}$ to the set of n motor inputs $\widetilde{\mathbf{m}}_{*,U}$ that elicited them. We now find the weighted average of these n adjusted motor inputs, as in eq. (4),

$$\phi_n(\widetilde{\mathbf{m}}_{*,U}) = \phi_n \left(\begin{bmatrix} \mathbf{m}_{*,U,1} & \dots & \mathbf{m}_{*,U,n} \end{bmatrix}^T \right) = \widehat{\mathbf{m}}_*. \tag{10}$$

Using this process, we can map every FS sensation observed during the FS-centered calibration, $\mathbf{f}_*$, to a personalized motor command $\widehat{\mathbf{m}}_*$. The complete adjustment for our data-driven approach is

$$\begin{aligned} \widehat{\mu}_D(\mathbf{f}_*) &= \phi_n(\alpha_{U,n}(\rho_n(\gamma(\mathbf{f}_*)))) = \phi_n(\alpha_{U,n}(\rho_n(\mathbf{d}_*))) \\ &= \phi_n(\alpha_{U,n}(\widetilde{\mathbf{d}}_{*,U})) = \phi_n(\widetilde{\mathbf{m}}_{*,U}) = \widehat{\mathbf{m}}_*, \end{aligned} \tag{11}$$

which can be substituted for $\mu(\cdot)$ in eq. (3) to give the full rendering algorithm with data-driven personalization. In this work, we consider $n = 8$, as it was proven to provide the best rendering performance [12].

This first approach for rendering personalized haptic cues is quite general and easy to use, as it is completely data-driven and does not require any additional knowledge about the device or the user's fingertip. All the information this approach needs is retrieved during two data collection processes; we expect this approach to inherently account for the stiffness and elasticity of the fingertip to render similar forces and/or pressure distributions to different fingertips. On the other hand, this approach requires that a rich haptic sensor in placed in the moving platform during data collection and that each user undergoes one data collection routine.

B. Geometric personalization

Our second approach uses the geometry of the target fingertip to personalize the FS-centered lookup table. This approach's objective is to adjust the behavior of the mobile platform so as to replicate on the user the *deformation* generated on the FS's rubber surface during data collection. Similar to Sec. III-A, we define a new mapping function

$$\widehat{\mu}_G(\mathbf{f}_*) = \varepsilon(\mu(\mathbf{f}_*)) = \varepsilon(\mathbf{m}_*) = \widehat{\mathbf{m}}_*, \tag{12}$$

where $\varepsilon(\cdot)$ adjusts each motor input registered during the FS-centered data collection. The complexity of $\varepsilon(\cdot)$ is arbitrary and depends on the information available about the target finger. Here we employ a simple 1-DoF model of the fingertip, which we simply define by a sphere of radius r. As discussed in Sec. VII, we plan to consider more complex geometric approximations in the future.

We start by running an FS-centered data collection, similar to Secs. II-B and III-A, with the FS placed inside the device as in Fig. 1a. No additional device-mounted sensor is needed for this approach. Let us consider a representative configuration of the device, with the mobile platform tilted upward on the left and pressing on the sensor. Fig. 5a shows a 2D front view of the device in this configuration during data collection, while Fig. 5b shows a 2D front view of the device in the target personalized configuration when worn by the user. Let S_0 be the reference frame fixed on the centroid of the static platform and ($\mathbf{x_0}$, $\mathbf{y_0}$, $\mathbf{z_0}$) be its unit vectors. All the following positions are referenced with respect to S_0 unless otherwise stated. Similarly, let S_1, with unit vectors ($\mathbf{x_1}$, $\mathbf{y_1}$, $\mathbf{z_1}$), be the reference frame fixed on the centroid of the mobile platform and let $\mathbf{p}_c$ be the position of this centroid. We approximate the FS with a sphere of radius $r_F = 7.5$ mm, centered at $\mathbf{p}_F$. For each device configuration, our objective is to adjust the position of the platform relative to the user's fingertip so as to render to the user (Fig. 5b) the same absolute deformation applied to the FS (Fig. 5a). Let $\widehat{S}_1$ be the reference frame fixed on the adjusted mobile platform's centroid, and let $\hat{\mathbf{p}}_c$ be the position of this centroid. We approximate the user's fingertip with a sphere of radius r_U, centered at $\mathbf{p}_U$. We assume that the FS and user fingertip are positioned such that $\mathbf{p}_F = \mathbf{p}_U$. In the representative case of Fig. 5, the platform needs to be moved up to ensure a match in the target deformation because $r_U < r_F$, but the following procedure can be applied to a fingertip of any size.

Since our data collection provides a lookup table of sensations $\mathbf{f}_*$ elicited by certain motor actions $\mathbf{m}_*$, we first convert each $\mathbf{m}_*$ to the corresponding mobile platform position and orientation, given by $\mathbf{p}_c$ and S_1, respectively. To convert between motor commands and mobile platform pose, we assume the three cables remain parallel to the $\mathbf{z_0}$ axis and define the contact surface as the plane that intersects the bases of these three cables. However, the equations in this section hold for any device, so long as the forward and inverse kinematics can be computed. Next, we calculate the point $\mathbf{p}_o$ at which the undeformed surface of the FS is parallel to our mobile platform,

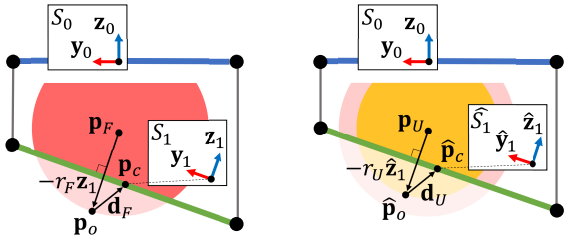

(a) Device worn by the FS sensor during data collection.

(b) Device worn by a user with a fingertip smaller than the FS.

Fig. 5. 2D device schematic (front view) of a representative configuration. The blue segment represents the static platform of the device, the green segment the mobile platform, the red disk the fingertip-shaped sensor (FS), and the yellow disk the subject's fingertip. To match the same deformation (i.e., $\mathbf{d}_U = \mathbf{d}_F$), the mobile platform needs to be moved up from its position in (a).

$$\mathbf{p}_o = \mathbf{p}_F - r_F \cdot \mathbf{z}_1. \tag{13}$$

We are then able to estimate how much and in which direction the mobile platform deforms the sensor,

$$\mathbf{d}_F = \mathbf{p}_c - \mathbf{p}_o. \tag{14}$$

The magnitude of this deformation is zero when the platform barely touches the sensor, and it increases as the platform applies more pressure. To recreate the same deformation as was rendered to the FS, we define our desired finger deformation $\mathbf{d}_U = \mathbf{d}_F$, and we estimate the orientation and position of the centroid of the adjusted platform,

$$\widehat{S}_1 = S_0, \quad \hat{\mathbf{p}}_c = \mathbf{p}_U - r_U \cdot \hat{\mathbf{z}}_1 + \mathbf{d}_U. \tag{15}$$

Finally, we convert our adjusted mobile platform orientation and position into adjusted motor inputs $\hat{\mathbf{m}}_*$. By applying this procedure to each element $\mathbf{m}_*$ registered during the data collection, we can generate a new personalized lookup table.

This second approach for rendering personalized haptic cues is rather fast and easy to implement, as it does not require any additional sensor on the mobile platform, and more importantly it does not require the user to carry out any data collection process. Moreover, it is quite flexible, as it can be implemented with arbitrarily complex fingertip models. However, of course, this approach is only as good as the fingertip approximation chosen and the model of the device employed. This preliminary fingertip approximation is entirely geometric in nature, and thus it does not account for the stiffness of the fingertip, which almost certainly varies between a sensor and a user. We expect this approach to be most beneficial for light contact, where relatively small fingertip deformations are required. In Sec. VII, we discuss our future plans along this direction.

IV. Objective Evaluation

We first quantitatively evaluated the performance of our personalization approaches on six sensorized rubber fingertips.

We built two fingertip-like casts in addition to the one we used for the FS, following the same procedure presented in Sec. II-A. One is 13% smaller than the FS and has a spherical tip with radius 6.5 mm, and the other is 13% larger than the FS and has a spherical tip with radius 8.5 mm. We also constructed three casts of the authors' fingertips using a slightly different procedure that is shown in Fig. 6. We approximate each human cast with a sphere of radius r, defined as the distance from the middle of the rigid core to the bottom of the fingertip. We measured radii of 6.5 mm, 8 mm, and 10 mm for the three casts of human fingertips. Although they have mechanical properties that are not identical to those of human fingertips, we believe these rubber fingertips can provide a preliminary and objective evaluation of how our personalization approaches affect rendering

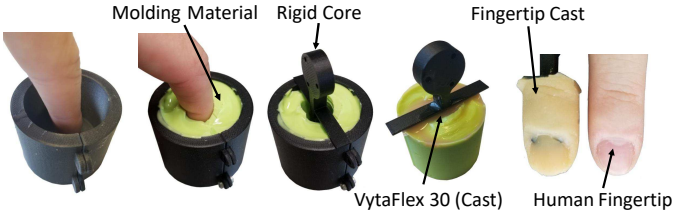

Fig. 6. The process of creating a cast of a human fingertip. We first make a mold out of Kulzer's Flexitime Correct Flow; then we insert a rigid core and fill the void with Smooth-On VytaFlex 30 to make the fingertip cast. The rigid core is later attached to a Nano17, as in Fig. 3b, creating a sensor that outputs a six-element vector of the forces and torques acting on the fingertip.

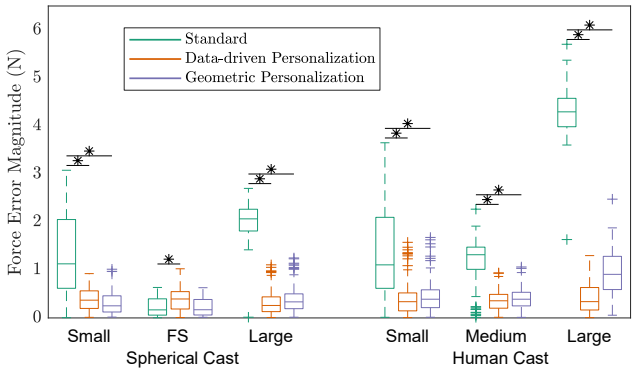

Fig. 7. Objective evaluation results. Box plots of rendering errors for each combination of fingertip cast and rendering approach. For each target cue, the error is defined as the magnitude of the difference between the force component of the target sensation, $\mathbf{f}$, and the force rendered to the test fingertip. Asterisks denote differences that are statistically significant, with $p < 0.0001$.

error. Finally, each of these six rubber fingertips can be attached to a Nano17 sensor (similar to Fig. 3b) and inserted into our fingertip device (similar to Fig. 2a).

Next, we built an FS-centered lookup table, as described in Sec. III. To do so, we placed the FS inside the device and the DS below the mobile platform, as shown in Fig. 2a. Then, we moved the motors to 13^3 (2,197) different configurations $\mathbf{m}_*$ that were evenly distributed throughout the entire motor space of the device. Each motor pose was commanded for one second, and then the six-dimensional outputs of both sensors ($\mathbf{f}_*$, $\mathbf{d}_*$) were recorded and averaged over a 0.2 s window (200 samples). For testing the data-driven approach of Sec. III-A, we also generated a user-centered lookup table for each fingertip cast. To limit this process to ten minutes, we tested a set of 7^3 (343) motor configurations $\mathbf{m}_{*,U}$, saving each resulting DS sensation $\mathbf{d}_{*,U}$. These motor inputs were again evenly distributed throughout the device's motor space. Finally, we generated a set of simulated remote sensations to be rendered by our fingertip device. To do so, we placed the FS into the device and recorded the sensations $\mathbf{f}$ for 100 configurations of the mobile platform that made contact with the FS and were randomly distributed throughout the device's motor space.

We evaluated each rendering approach – standard (Sec. II-B), data-driven personalization (Sec. III-A), and geometric personalization (Sec. III-B) – on each of the six rubber fingertips. As a measure of performance, we consider the magnitude of the difference between the force component of the target sensation $\mathbf{f}$ and the force actually rendered to the fingertip. This objective evaluation was inspired by a similar one presented in [12], in which the authors showed that a low error in such objective evaluation leads to a high perceptual performance during human-subject studies.

The mean force magnitude rendered to the FS across all target cues was 1.72 N. Using the standard approach, the mean forces rendered to the cast fingertips ranged from 0.41 N for the small spherical cast

to 5.99 N for the large human casts.

Cues rendered to the FS using the standard method had a median force error magnitude of 0.17 N. Rendering the target sensations $\mathbf{f}$ to the FS requires no personalization, as the FS-centered lookup table is already built for the FS. Therefore, this error represents our baseline (i.e., the lowest error we can expect even with ideal personalization). The rendering error associated with the standard approach was significantly smaller for the FS than for all other fingertips, as expected. The errors associated with each of the six cast fingertips and each of three rendering approaches are shown in Fig. 7.

For all of the tested cast types, there was a significant effect of the rendering approach (Friedman statistical test with $p < 0.0001$ for all cast types). The post-hoc analysis showed that the data-driven and geometric personalizations significantly reduced the error compared to the standard approach for all of the fingertip casts other than the FS (Wilcoxon matched pairs signed rank tests with $p < 0.0001$ while Bonferroni correction required $p < 0.0028$). Furthermore, we compared the two personalization methods across all conditions, and we found the force error magnitude of the data-driven approach was significantly smaller than that of the geometric one (Wilcoxon matched pairs signed rank test, W = 22682, $p = 0.0076$). The difference was especially large for the cast of the large human fingertip, for which the geometric personalization had much higher errors than in other conditions.

V. Human-Subject Evaluation

We also performed a human-subject study. The experimental setup was nearly identical to that presented in Sec. IV and was inspired by [12], in which participants rated the similarity between tactile interactions they saw and tactile interactions they felt. To generate the user-centered lookup table, we asked the participants to wear the fingertip device on their right index finger, as in Fig. 2b. For the sake of their comfort, we reduced the set of motor configurations $\mathbf{m}_{*,U}$ to 5^3 (125), which takes roughly five minutes to collect. Subjects were isolated from external noise through a pair of headphones, and their vision of their fingertip in the device was blocked by a wooden panel. Then, we placed a second device with the FS inside, as in Fig. 2a, right in front of them. During each trial, we simultaneously rendered one sensation to the subject's hidden finger (H) and one to the visible FS (V). Each sensation was maintained until the user rated the similarity of the cue they felt on their fingertip to the one they saw on the FS. After that, both devices returned to a neutral pose with no contact. The rating was given on a number pad that ranged from 1 to 9, where a score of 1 meant "very different" and a score of 9 meant "very similar".

We selected ten target sensations from the original 100 in Sec. IV that delivered forces of less than 1 N to the FS, so as to evaluate our methods on light-contact interactions that are more difficult to render. Each cue applied on the visible FS was rendered using the original motor commands associated with the target sensation, while each cue applied on the hidden fingertip was rendered by feeding the target sensation into one of three rendering approaches and using the adjusted motor commands. We rendered each of the ten sensations twice using each of the three rendering approaches, for a total of 60 comparisons per subject. In addition to these, we also asked the subjects to compare two cues in which we rendered a very strong contact on the FS (all motors pulling the platform up) and no contact at all on the user's fingertip (V1/H0), and two cues with no contact on the FS and a very strong contact at the fingertip (V0/H1). These four comparisons are useful to understand how users judge sensations that are clearly different from each other. Eight females and five males participated in this study, which was approved by the Penn IRB under protocol 834168. All subjects gave informed consent. One participant

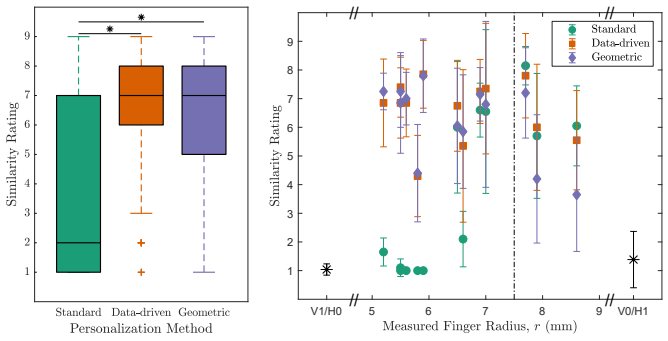

(a) Box plot of all ratings. (b) Similarity ratings for all 13 participants.

Fig. 8. Human-subject study results. (a) Boxplots for the ratings of the three rendering methods across all trials. Asterisks denote differences that are statistically different, with $p < 0.0001$. (b) Each point represents the mean rating of 20 trials for a single participant, and the bars represent standard deviations. The vertical dashed line at 7.5 mm shows the FS radius. The two asterisks give the means and standard deviations of ratings for the conditions with strong FS contact and no user's fingertip contact (V1/H0), and no FS contact with strong fingertip contact (V0/H1) across all participants.

did the experiment twice due to a calibration error in the first run; we report only the second data set.

In Fig. 8a, we see that across all trials, the similarity rating was significantly affected by the rendering approach (Friedman statistical test: n = 260, Q(3) = 118.7, $p < 0.0001$). The mean ratings for the standard, data-driven, and geometric methods were 3.7, 6.6, and 6.3, respectively. A post-hoc analysis further showed that ratings were significantly lower for the standard approach compared to the other two (Wilcoxon matched-pairs signed-ranked test: $p < 0.0001$), while the data-driven and geometric approaches did not significantly differ. In Fig. 8b we see that the performance of the standard approach tends to degrade as the difference between the radius of the subject's finger and FS (7.5 mm) increases. The standard approach performs worst for small fingertips, for which some trials resulted in a clear contact on the FS and no contact at all on the user's fingertip.

VI. Discussion

Both evaluations confirm that the performance of the standard rendering algorithm significantly degrades as the fingertip starts to differ from the sensor FS used for building the lookup table.

As expected, the standard technique of Sec. II-B renders contacts on the FS very well, with a median error of less than 0.2 N, confirming the results of [25]; this technique also shows good performance in rendering contacts on human fingertips that are sized similar to the FS. In these cases, rendering personalized cues provides no benefit over the standard method. However, as the difference between the target fingertip and the FS increases, the performance of the standard method degrades. The standard approach performed significantly worse for all the rubber fingertips other than the FS, with measured force errors as large as 5 N for the largest cast fingertip. Similarly, human subjects with fingers larger or smaller than the FS gave lower ratings. We note that the standard approach performs worse for smaller fingers than for larger fingers, since smaller fingers are often not contacted at all, causing several subjects to give all 20 standard trials a rating of one.

The results also show the overall viability and effectiveness of our personalization approaches. For our rubber fingertips other than the FS, both personalization approaches are able to significantly reduce the rendering error. For the human subjects, we see in Fig. 8a that both the data-driven and geometric personalization methods were rated significantly higher than the standard approach across trials.

However, our results also suggest that there are areas of improvement, especially for our geometric personalization. For the large rubber

human fingertip, the geometric personalization leads to significantly larger errors than the data-driven one. We also notice that the geometric personalization method tends to receive lower ratings from subjects with larger fingertips. These results suggests that the true geometry of these fingertips may not be well represented by our one-dimensional model. Moreover, a geometric model cannot capture biomechanical variations, such as the elasticity and anisotropy of the skin. For human fingertips that are larger than the FS, we expect the geometric approach to reduce fingertip deformation. However, if these fingers are also less stiff than the FS, then the smaller deformations may result in unrealistically small forces. Thus, updating our fingertip model to account for finger mechanics may improve our personalization approach. These mechanical characteristics are inherently taken into account by the data-driven personalization, as it focuses on the contact forces applied by the end-effector. As such, the data-driven approach receives consistently high ratings regardless of finger radius, with all participants giving it mean ratings greater than five.

VII. Conclusion and Future Work

While wearable and fingertip haptic devices are gaining increasing popularity, little work has been dedicated to the important issue of adapting devices and algorithms to fingertips of different sizes and shapes. This work presented the first effort in devising personalized haptic rendering techniques for fingertip haptics. We presented two personalization techniques, the first of which is purely data driven. It requires an additional sensor on the platform during the data collection phase, and it requires each user to undergo a data collection procedure. However, it does not need any knowledge about the fingertip or device characteristics. The second technique aims at matching the deformation generated on the FS sensor during data collection, for which a geometric model of the fingertip is needed. However, it does not require any additional sensor, and it does not require the user to undergo a data collection routine. Overall, our results suggest that both approaches can effectively personalize tactile interactions rendered by a haptic device to fingertips of different shapes and sizes. Although we employed a specific fingertip device and sensor to present and evaluate our personalization techniques, the same approaches can be applied to any other similar haptic system.

This paper serves as a starting point for optimizing the rendering of haptic interfaces for different fingertips, and we plan to expand these methods in the future, as our data-driven and geometric personalization approaches have many parameters that can be further explored. For the geometric personalization, we hope to implement higher-dimensional geometric models of the user's fingertip, such as generating a point cloud from a 3D scan, or using a mechanical model that details the relationship between force and deformation. For the data-driven personalization, we want to examine the effect of weighting functions, number of nearest neighbors, and lookup table size on the rendering error. Moreover, we hope to evaluate both approaches with different sensors, such as a BioTac, and devices that have more degrees of freedom or can render different tactile sensations, such as shear. Finally, it would be interesting to extend such personalization approaches to also consider differences in the relative positioning of the fingertip with respect to the device end-effector.

References

[1] C. Pacchierotti, S. Sinclair, M. Solazzi, A. Frisoli, V. Hayward, and D. Prattichizzo, "Wearable haptic systems for the fingertip and the hand: taxonomy, review, and perspectives," *IEEE Trans. Haptics*, vol. 10, no. 4, pp. 580–600, 2017.

[2] K. Dandekar, B. I. Raju, and M. A. Srinivasan, "3-D finite-element models of human and monkey fingertips to investigate the mechanics of tactile sense," *J. Biomechanical Engineering*, vol. 125, no. 5, pp. 682–691, 2003.

[3] P. W. Johnson and J. M. Blackstone, "Children and gender-differences in exposure and how anthropometric differences can be incorporated into the design of computer input devices," *Scandinavian Journal of Work, Environment & Health*, pp. 26–32, 2007.

[4] A. Courtney and M. Ng, "Hong Kong female hand dimensions and machine guarding," *Ergonomics*, vol. 27, no. 2, pp. 187–193, 1984.

[5] O. F. Obi, "Hand anthropometry survey of rural farm workers in south-eastern Nigeria," *Ergonomics*, vol. 59, no. 4, pp. 603–611, 2016.

[6] S. N. Imrhan, M. Sarder, and N. Mandahawi, "Hand anthropometry in Bangladeshis living in America and comparisons with other populations," *Ergonomics*, vol. 52, no. 8, pp. 987–998, 2009.

[7] H. E. Wheat, L. M. Salo, and A. W. Goodwin, "Human ability to scale and discriminate forces typical of those occurring during grasp and manipulation," *J. Neuroscience*, vol. 24, no. 13, pp. 3394–3401, 2004.

[8] D. Gueorguiev, E. Vezzoli, A. Mouraux, B. Lemaire-Semail, and J.-L. Thonnard, "The tactile perception of transient changes in friction," *J. Royal Society Interface*, vol. 14, no. 137, 2017.

[9] E. R. Serina, C. D. Mote Jr., and D. Rempel, "Force response of the fingertip pulp to repeated compression - effects of loading rate, loading angle and anthropometry," *Journal of Biomechanics*, vol. 30, no. 10, pp. 1035–1040, 1997.

[10] D. T. V. Pawluk and R. D. Howe, "Dynamic lumped element response of the human fingerpad," *Journal of Biomechanical Engineering*, vol. 121, no. 2, pp. 178–183, 1999.

[11] C. Pacchierotti, D. Prattichizzo, and K. J. Kuchenbecker, "Cutaneous feedback of fingertip deformation and vibration for palpation in robotic surgery," *IEEE Trans. Biomedical Engineering*, vol. 63, no. 2, pp. 278–287, 2016.

[12] ——, "Displaying sensed tactile cues with a fingertip haptic device," *IEEE Trans. Haptics*, vol. 8, no. 4, pp. 384–396, 2015.

[13] G. Robles-De-La-Torre and V. Hayward, "Force can overcome object geometry in the perception of shape through active touch," *Nature*, vol. 412, no. 6845, pp. 445–448, 2001.

[14] A. W. Goodwin and H. E. Wheat, "Magnitude estimation of contact force when objects with different shapes are applied passively to the fingerpad," *Somatosensory & Motor Research*, vol. 9, no. 4, pp. 339–344, 1992.

[15] A. M. Smith, G. Gosselin, and B. Houde, "Deployment of fingertip forces in tactile exploration," *Experimental Brain Research*, vol. 147, no. 2, pp. 209–218, 2002.

[16] A.-S. Augurelle, A. M. Smith, T. Lejeune, and J.-L. Thonnard, "Importance of cutaneous feedback in maintaining a secure grip during manipulation of hand-held objects," *J. Neurophysiology*, vol. 89, no. 2, pp. 665–671, 2003.

[17] M. Maisto, C. Pacchierotti, F. Chinello, G. Salvietti, A. De Luca, and D. Prattichizzo, "Evaluation of wearable haptic systems for the fingers in augmented reality applications," *IEEE Trans. Haptics*, vol. 10, no. 4, pp. 511–522, 2017.

[18] E. M. Young and K. J. Kuchenbecker, "Implementation of a 6-DOF parallel continuum manipulator for delivering fingertip tactile cues," *IEEE Trans. Haptics*, vol. 12, no. 3, pp. 295–306, 2019.

[19] D. Prattichizzo, F. Chinello, C. Pacchierotti, and M. Malvezzi, "Towards wearability in fingertip haptics: a 3-DoF wearable device for cutaneous force feedback," *IEEE Trans. Haptics*, vol. 6, no. 4, pp. 506 – 516, 2013.

[20] D. Leonardis, M. Solazzi, I. Bortone, and A. Frisoli, "A 3-RSR haptic wearable device for rendering fingertip contact forces," *IEEE Trans. Haptics*, vol. 10, no. 3, pp. 305–316, 2016.

[21] M. Solazzi, A. Frisoli, and M. Bergamasco, "Design of a novel finger haptic interface for contact and orientation display," in *Proc. IEEE Haptics Symposium*, 2010, pp. 129–132.

[22] R. M. Khurshid, N. Fitter, E. Fedalei, and K. J. Kuchenbecker, "Effects of grip-force, contact, and acceleration feedback on a teleoperated pick-and-place task," *IEEE Trans. Haptics*, vol. 10, no. 1, pp. 40–53, 2016.

[23] N. Wettels and G. E. Loeb, "Haptic feature extraction from a biomimetic tactile sensor: force, contact location and curvature," in *Proc. International Conf. Robotics and Biomimetics*, 2011, pp. 2471–2478.

[24] C. Pacchierotti, *Cutaneous haptic feedback in robotic teleoperation*, ser. Springer Series on Touch and Haptic Systems. Springer, 2016.

[25] C. Pacchierotti, A. Tirmizi, and D. Prattichizzo, "Improving transparency in teleoperation by means of cutaneous tactile force feedback," *ACM Transactions on Applied Perception (TAP)*, vol. 11, no. 1, p. 4, 2014.